Eur. Phys. J. D (2010)
DOI: 10.1140/epjd/e2010-10195-x

THE EUROPEAN PHYSICAL JOURNAL D

Regular Article

Collisions between a single gold atom and 13 atom gold clusters: an ab initio approach

F. Muñoz[1,3], J. Rogan[2,3], G. García[1,3], M. Ramírez[2,3], J.A. Valdivia[2,3], R. Ramírez[1,3], and M. Kiwi[1,2,3,a]

[1] Facultad de Física, Pontificia Universidad Católica de Chile, Casilla 306, 7820436 Santiago, Chile
[2] Departamento de Física, Facultad de Ciencias, Universidad de Chile, Casilla 653, Santiago, Chile
[3] Centro para el Desarrollo de la Nanociencia y la Nanotecnología, CEDENNA, Avda. Ecuador 3493, Santiago, Chile

Received 14 April 2010 / Received in final form 1st July 2010
Published online 3rd December 2010 – © EDP Sciences, Società Italiana di Fisica, Springer-Verlag 2010

Abstract. Collision processes between a single gold atom and a gold cluster are investigated by means of ab initio techniques. The targets we consider are minimum energy 13 gold atom clusters. The kinetic energy of the projectile and its impact parameter are chosen within a range such that the three regimes we are mainly interested in studying (fusion, scattering and fragmentation) are realized. The results of the collision processes are treated using density functional theory molecular dynamics (DFT-MD), analyzed in detail, and compared with previous work, which was carried out using phenomenological potentials and classical molecular dynamics. The differences between classical MD and DFT-MD are quite significant.

1 Introduction

The study of nanostructures is a subject of widespread attention for scientists and industry alike [1]. In particular, experimental and theoretical physicists and chemists have, in recent years, created the tools and equipment to develop a reliable and relevant description and understanding of nanoparticles. On the other hand, the interest in our focus of attention, namely gold clusters, is long dated since they have been used for centuries in colloidal suspension (to stain glass). The interest in the physics and chemistry of gold nanoclusters continues to this date; as an example we mention the recent studies of catalytic activity of gold nanoclusters in the selective CO oxidation [2,3].

On the theoretical front ab initio procedures are now capable of providing incisive insights into the properties of both bulk and nano-sized systems. In addition, novel and sophisticated nanostructure fabrication, manipulation and measurement techniques have given impetus to experiment, and reliability to a large wealth of experimental data, which in time has led to a significant amount of technological applications and a large variety of devices. All in all the activity in the nanoworld has received a strong stimulus, with nanoclusters playing an important role because of their special properties, quite different from the ones the same elements exhibit in the bulk, and because they can be used as building blocks of novel nanostructured materials and devices.

Several years ago some of the authors of this paper already tackled the problem of gold cluster collisions using classical molecular dynamics [4] in combination with Foiles et al. [5] phenomenological potentials. In the meantime both the increase in the number crunching capacity of present day computers and the improvement and refinement of the available first principle codes, has allowed us to partially reexamine our own results using ab initio methods. In principle, one does expect ab initio procedures to be the definitive tool to handle this type of cluster collisions; however, it is still not feasible (or at least not practical) to implement such ab initio calculations for large clusters. Andersen et al. [6–8], not so long ago, provided an exhaustive review of the literature which covers, among many other topics, description of ab initio treatments and analysis of its results, ranging from the simplest case: a proton colliding a hydrogen atom ($H^+ + H$), all the way to collisions between clusters of strontium and noble gas clusters.

More recently, collisions of rather large clusters have been simulated by means of classical molecular dynamics in combination with Lennard-Jones, and also with more elaborate phenomenological potentials. Kalweit and Drikakis [9] used Lennard-Jones potentials to investigate the collision dynamics of clusters as large as 11 000 atoms to probe these systems near the hydrodynamic limit (droplet collisions). Mariscal et al. [10] used embedded atom type potentials to study collisions of two different chemical species to investigate the formation of binaries (Pt-Au, Pd-Au and Cu-Ag). Alamanova et al. [11] implemented a similar scheme to calculate the dynamics of Cu-Cu nanocluster collisions.

Our present aim is an ab initio study of the collision of a single gold atom with a Au_{13} cluster target, using density functional theory (DFT) techniques. Our goal is to obtain a detailed quantum mechanical description of the dynamics of the collision process and to contrast this dynamics with the results we obtained previously with phenomenological potentials [4].

[a] e-mail: mkiwi@puc.cl

This paper is organized as follows: after this introduction, the method and computational details are presented in Section 2. Next the choice, characteristics and specification of the target cluster are given in Section 3. The energy and impact parameter dependence of the collision are described and analyzed in Section 4, while the impact dynamics is discussed in Section 5. In Section 6 we discuss the consequences of incorporating magnetic effects. Finally, in Section 7, we draw conclusions and close this paper.

2 Method and computational details

Gold cluster collisions are simulated using the DFT formalism [12,13] as implemented in the VASP code [14–16]. In order to avoid self-interactions, or even worse, spurious interactions between fragments scattered after the collision, we use the largest possible simulation cell (i.e. compatible with our computational resources, that is a cube of sides close to 20 Å). In addition, we treat the fragments separately when their interaction becomes negligible. PAW pseudopotentials [17] and PBE [18–20] for the exchange-correlation, are used. The energy cutoff was set to 230 eV. The targets we choose are Au_{13} clusters. Fortunately, these gold clusters, as well as different size ones, have been widely studied and reported in the literature at the DFT level [21–33], and we made sure that our initial set of parameters yield an adequate description of them.

Although our targets are nonmagnetic the atomic rearrangement during the collision process can give rise to magnetic behavior. Thus, we carried out some spin-polarized calculations (explained in detail below) in order to check the relevance of magnetic effects in our calculations. However, in this context, they turned out to be negligible and thus we only report detailed results for non spin-polarized configurations.

The collisions are setup as follows: first we choose a proper collision target (i.e. a cluster in the minimum energy configuration) which is positioned at the origin of the simulation box. The projectile is located some distance away from the cluster and impinges orthogonally on the target. We limit our attention to Au_{13} clusters aligned in such a way as to maximize their cross sections. The impact parameter b is measured in Å units relative to the cluster center of mass, and is positive (negative) above (below) the center of mass of the clusters illustrated in Figure 1. The target, which will be described in detail in Section 3, has no initial center of mass velocity and no vibrational energy (i.e. $T = 0$ K). Next, a gold atom is placed at ≈8.5 Å from the nearest target atom. The projectile carries a kinetic energy E_k and flies toward the target with an impact parameter b, for a time of 2 ps, conserving the total energy (i.e. the simulation is carried out in the microcanonical ensemble). This way the system initially evolves freely during 2 ps, just constrained by energy conservation.

After the collision takes place, and depending on the values of both E_k and b, we contemplate one of the following three scenarios: fusion of target and projectile, target fragmentation, or projectile scattering. It may be worth mentioning that at least another possibility does exist: evaporation, but the simulation times involved in this physical process are beyond the scope of our computational resources. Certainly, after the collision takes place the target is left in an excited (high temperature) state and to systematize our analysis of the data it is necessary to get rid of this excess excitation energy. Thus, finally we simulate a radiation process, or cooling down of the system after collision, by linearly rescaling the atomic velocities until they reach room temperature, which takes an additional time of around 3 ps.

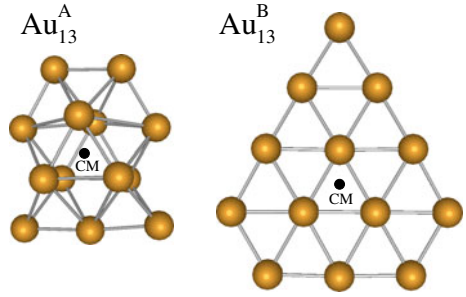

Fig. 1. (Color online) The Au_{13}^{A} and Au_{13}^{B} configurations used in our calculations. The projectile is located some distance away from the plane that is illustrated and impinges orthogonally on the target. The impact parameter b is measured in Å units relative to the cluster center of mass (CM), and is positive (negative) above (below) CM.

3 Target cluster

Our first task, in order to carry out a proper simulation, is to select a physically realistic collision target. Thus, we search for the minimum Au_{13} configuration by a method described elsewhere [34], obtaining the structure denoted as Au_{13}^{A} in Figure 1 as the most stable conformation. However, we also decided to use the lowest energy configuration of Au_{13} reported in the literature [31–33], which corresponds to Au_{13}^{B} (see Fig. 1), and has the peculiarity of being planar and lies ≈0.5 eV below the Au_{13}^{A} energy. Since at this time the Au_{13}^{B} conformation is the putative groundstate we focused most of our efforts on it.

An additional issue of interest is to determine the differences between a collision of a gold atom with a planar and a 3D target. Thus, we carry out simulations for both type of targets (i.e. Au_{13}^{A} and Au_{13}^{B} clusters). It should be mentioned that recent studies on Au clusters, including spin-orbit coupling terms, showed that relativistic effects do not change the relative stability among planar and 3D Au clusters [31,32]. As can be seen in Figure 1 both targets are not rotationally invariant. Thus, in order to avoid an excessively large number of time consuming calculations, we limited our attention to Au_{13} clusters aligned in such a way as to maximize their cross sections. The magnetic moment of both Au_{13}^{A} and Au_{13}^{B} is $\mu = 1\ \mu_B$. However, if the calculation is carried out for the $\mu = 0$ state the energy difference with the $\mu = 1\ \mu_B$ state turns out to be tiny.

4 Energy and impact parameter dependence

The dependence of the scattering process on the impact parameter b and the kinetic energy E_k of the projectile, are illustrated in Figure 2 for the Au_{13}^{B} configuration and in Figure 3 for the Au_{13}^{A} configuration. As mentioned above we limit our interest to three scenarios: fusion, scattering and fragmentation. Other outcomes are certainly possible but for the time being we just consider these three regimes which are the most likely ones. In both figures these three regimes (fusion, scattering and fragmentation) are enclosed by red (continuous), blue (short dash) and green (long dash) frames, respectively.

When the projectile impinges on the Au_{13}^{B} configuration it is apparent that, within the parameter space that we investigated, fusion (red continuous frame) is the dominant collision outcome and it occurs for a large combination of b and E_k values. Even for $b = 4$ Å and $E_k = 9$ eV an isolated fusion event is observed in an otherwise fragmentation dominated region. This is in contrast with the classical molecular dynamics results summarized in Figure 7 of the paper of Rogan et al. [4], where a much stronger tendency towards fragmentation is quite apparent. Upon inspection of the movies of the DFT collision process one realizes that charge transfer between the atoms plays a key role. Actually, one observes atoms "trying" to abandon the cluster but they are pulled back by electrostatic interactions. Thus, we conclude that a quantum description of the collision process is difficult to avoid.

Fragmentation (green long dash frame) is the second most frequent outcome, and it occurs preferentially for larger energies and for the projectile impinging in the vicinity of the center of mass of the cluster. In the fragmentation region of Figure 2 isolated black circles indicate that single atoms have broken away from the cluster. Two contiguous black circles indicate that a dimer is ejected. Illustrations of the outcomes of collision against the 0.5 eV higher energy 3D Au_{13}^{A} structure, given in Figure 3, show similar tendencies, i.e. fusion continues to be dominant, even more so than before. Scattering (blue short dash frame) instead is mainly the consequence of large impact parameter collisions and is of rather low occurrence. Moreover, the large variety of the resulting structures, illustrated in Figures 2 and 3, is quite remarkable and has important implications as a novel method to generate a bank of diverse configurations, in the process of searching for minimum energy structures [34].

In Figure 4 we illustrate the transfer of energy between the projectile and the Au_{13}^{B} target. Or, in other words, the efficiency of the fragmentation process as a way of cooling the cluster. In spite of the diversity of the results it is possible to draw several conclusions. For impact parameters $b = 6, 5, 1, -3, -4$ Å the fragmentation process is very effective, the projectile hits one of the cluster atoms head on and this atom is detached. This occurs mainly when the impact is with atoms located on the cluster perimeter, or when the projectile collides an atom head on and replaces it ($b = 1$).

In the rest of the cases fragmentation is not a simple instantaneous process; on the contrary, it implies the rearrangement of the atoms, mainly in the vicinity of the released fragment. This atomic reordering implies a significant amount of energy and fragmentation is insufficient to cool down the cluster. They correspond to rather large energy events, mainly the ones displayed on the right hand side of Figure 2. Finally, there are several cases for which there is no fragmentation, the projectile does not impinge head on on a particular atom, and what follows is projectile scattering and an energy redistribution all over the cluster.

In order to understand why the projectile energy E_k required to generate fragmentation is such a discontinuous function of the impact parameter b, we illustrate in Figure 5 how the process develops for several different b values. Except for minor changes the way the collision develops is rather insensitive to the magnitude of E_k. We observe that for $b = -2$ Å the force induced by the projectile is limited to basically two atoms, which in turn interact with their neighbors with the consequent spread of the energy over the whole cluster, thus avoiding fragmentation. If instead the projectile hits orthogonally the planar cluster just 1 Å lower ($b = -3$ Å) a force component is generated mainly on a single atom, which is significantly displaced perpendicular to the cluster plane, and consequently a kinetic energy of just 3 eV is sufficient to break up the cluster. This is similar to the $b = -4$ Å case, except that the in plane component effectively generates some buckling of the cluster which hinders fragmentation. Finally, for $b = -5$ Å a force towards the cluster center develops, which in turn generates a repulsion of the projectile that is scattered away from the cluster.

5 Impact dynamics

The potential energy during the evolution of the collision process in time is also a matter of interest and here we discuss two special, but quite representative, cases. As expected initially, when the projectile is far away from the target, the potential energy remains constant until projectile-cluster attraction becomes significant and there is an increase of the kinetic and a reduction of the potential energy, until the first minimum of Figure 6 is reached. Right afterward repulsion appears, since the projectile is too close to the target, and a significant increase of potential energy leads to a potential energy maximum. Next a slightly different dynamics for Au_{13}^{A} and Au_{13}^{B} takes place. While for the latter an atom is immediately expelled, the former cluster has to transfer forces to the second layer (second maximum in the figure) before expelling an atom and in this way reducing the potential energy of the system. However, this atom carries less kinetic energy than the incident projectile, while the energy difference sets the cluster in oscillation.

6 Magnetism and electronic states

Magnetism, and the underlying electronic structure that determines the characteristics of the magnetic behavior,

Fig. 2. (Color online) Au_{13}^{B} configurations after heat radiation. The impact parameter b, indicated at the left in Å units, is measured relative to the center of mass of the target. The kinetic energy of the projectile E_k is given at the top in eV units. The red (continuous), green (long dash) and blue (short dash) frames denote fusion, fragmentation and scattering, respectively. In the fragmentation region two isolated black circles indicate that two single atoms have broken away from the cluster. Two contiguous black circles indicate that a dimer is ejected. No black circle in the fragmentation region implies the ejection of one gold atom.

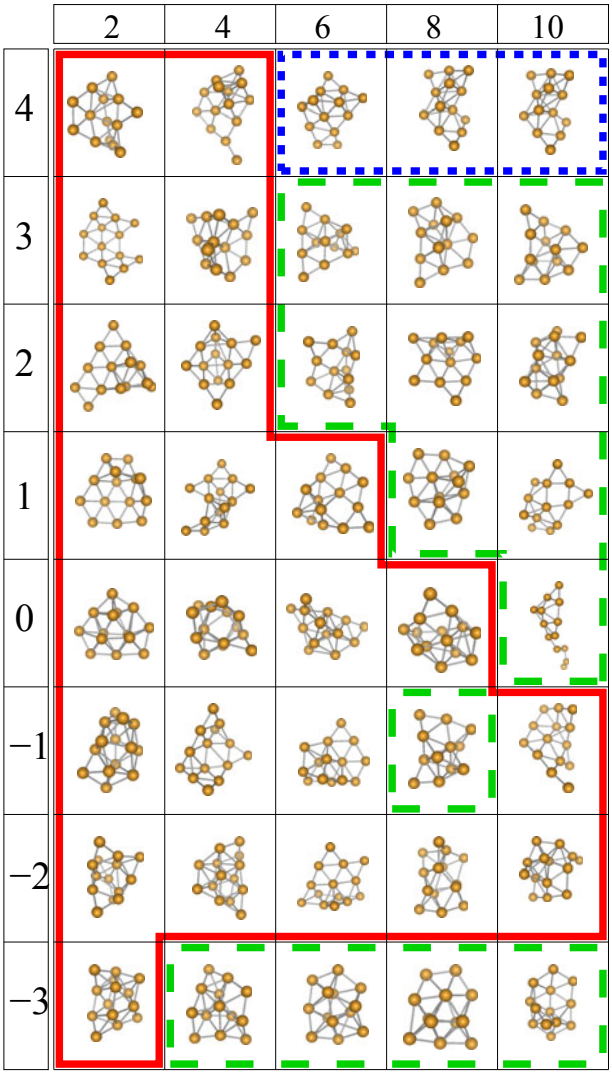

Fig. 3. (Color online) Au_{13}^{A} configurations after heat radiation. The impact parameter b, indicated at the left in Å units, is measured relative to the center of mass of the target. The kinetic energy of the projectile E_k is given at the top in eV units. The red (continuous), green (long dash) and blue (short dash) frames denote fusion, fragmentation and scattering, respectively.

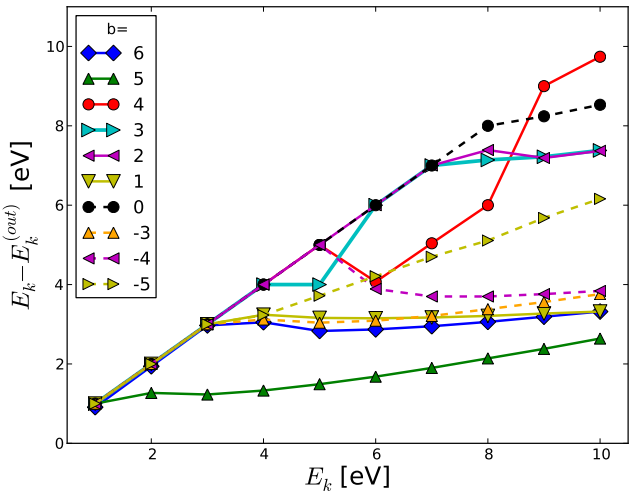

Fig. 4. (Color online) Projectile kinetic energy difference, before and after collision $E_k - E_k^{(out)}$, as function of the original kinetic energy E_k for the values of the impact parameter b indicated in the inset. The $b = -1$ and -2 cases are omitted since they correspond to simple fusion processes. The lines are a guide to the eye.

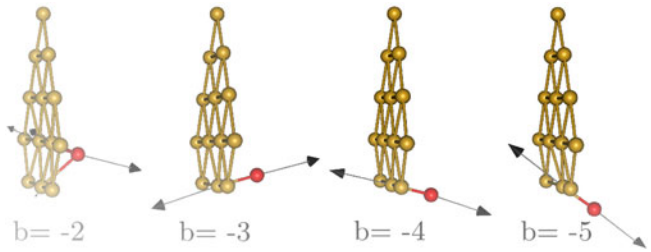

Fig. 5. (Color online) Details of the collision, with illustrations of the force vectors, for several values of the impact parameter b measured in Å units. The energy $E_k = 7$ eV, but the tendencies illustrated are only weakly dependent on E_k. The projectile (colored red) approaches the target from right to left. As can be seen by inspection of Figure 2 the $b = -2$ corresponds to fusion, $b = -3$ and $b = -4$ to fragmentation and $b = -5$ to scattering.

are also issues of interest. Thus, we carried out some spin polarized electronic state calculations to investigate the relevance that magnetic phenomena have in our context. In Figure 7 we display, for two representative cases, the magnetic moment μ of the whole system (target + projectile) as a function of time. The moment μ is carried either by the projectile or the expelled fragment. The values of E_k and b used here are the same as in Section 5. For Au_{13}^{A} we observe that the magnetic moment μ is quenched as the projectile reaches the vicinity of the cluster. But, when the atom is expelled μ recovers, apart from an irrelevant change of sign, its original magnitude. On the contrary, for Au_{13}^{B} we notice that the value of μ first increases and then is quenched by the interaction. However, the ejected atom looses completely its magnetic moment. In order to

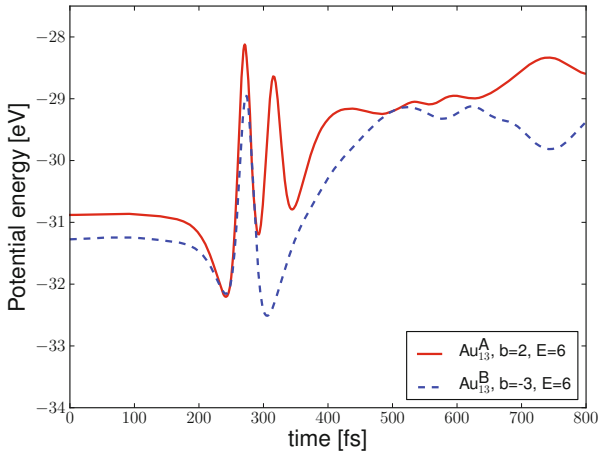

Fig. 6. Cluster potential energy versus time for two representative cases.

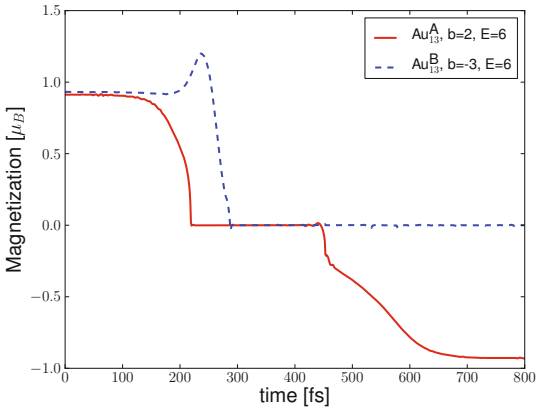

Fig. 7. Total magnetization μ before, during and after the collision, for two representative cases.

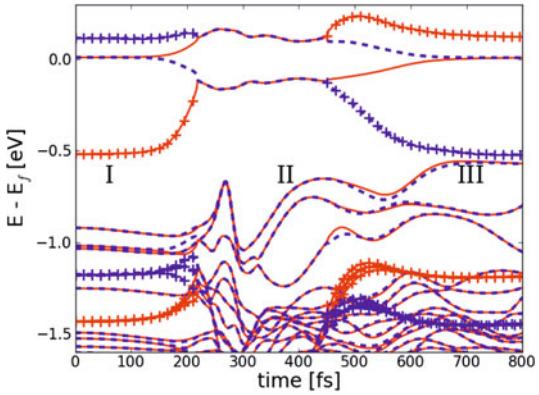

Fig. 8. (Color online) Energy levels before (I), during (II) and after the collision (III), for the Au^A_{13} cluster. The colors label the majority (red continuous) and minority (blue dashed) spin levels. In region I (III) the projectile (expelled atom) energy levels are denoted by + symbols.

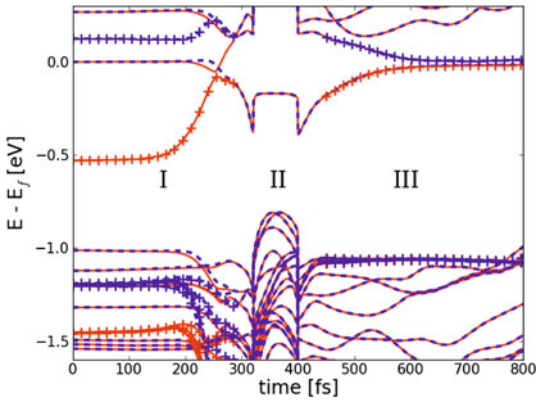

Fig. 9. (Color online) Energy levels before (I), during (II) and after the collision (III), font the Au^B_{13} cluster. The colors label the majority (red continuous) and minority (blue dashed) spin levels. In region I (III) the projectile (expelled atom) energy levels are denoted by + symbols.

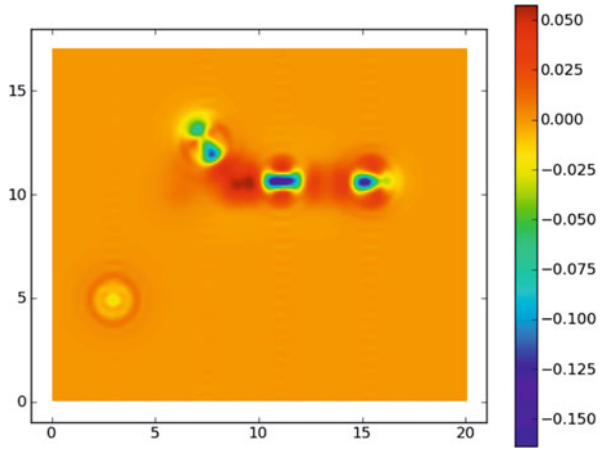

Fig. 10. (Color online) Charge redistribution $\Delta\rho(r) = \rho(r) - \rho^{\text{atomic}}(r)$, where ρ and ρ^{atomic} are the charges of the system after scattering and the superposition of the atomic charges of 14 non-interacting gold atoms, respectively. The Au^B_{13} atoms correspond to the horizontal blue spots, the fragmented atom is the orange-yellow circle on the lower left. The units of $\Delta\rho(r)$ are electrons per Å^3.

understand the contrast between these two different behaviors we plot, in Figures 8 and 9, the time evolution of the up and down energy levels, during the collision process both for Au^A_{13} and Au^B_{13}. At $t = 0$ (region I) both cases are similar, i.e. the projectile energy eigenvalues are the same, as expected. As the projectile approaches the target its energy eigenfunctions start to hybridize with the target ones and rapidly evolve during the collision process, denoted as region II in Figures 8 and 9.

Once the projectile leaves the vicinity of the cluster (region III) its energy eigenvalues approach constant values, but the Au^A_{13} and Au^B_{13} clusters exhibit a significantly different behavior during (region II) and after the collision takes place (region III). While the Au^A_{13} projectile eigenvalues are not altered by the collision (except for an irrelevant sign change), the Au^B_{13} projectile reaches new constant energy eigenvalues. The outgoing atom is scattered into an excited state while a strong s–d hybridization is preserved after the atom leaves the main cluster. This hybridization causes a complete degeneration of the energy levels thus generating a spurious nonmagnetic state. Also, in region II inspection of Figures 8 and 9 display quite different behaviors. While in Figure 8 a clear cut hybridization process is apparent, a sharp discontinuity is observed in Figure 9 which reflects the formation of a sort of virtual bound state between the projectile and an atom of the target. This energy is subsequently transferred to the rest of the atoms in the cluster, generating the energy oscillations observed in region III of Figure 9, accompanied by a significant increase of the HOMO-LUMO gap.

Clearly, the s–d hybridization here plays a central role, as already pointed out by Häkkinen et al. [33], which must be reflected in the charge rearrangement. To underline this point we have plotted, in Figure 10, the charge redistribution $\Delta\rho(r) = \rho(r) - \rho^{\text{atomic}}(r)$, where ρ and ρ^{atomic} are

the charges of the converged system after scattering and the superposition of the atomic charges of the 14 non-interacting gold atoms. The plane we have chosen is the one formed by the fragment, the projectile and the widest region of the Au_{13}^{B} cluster. We observe that the charge density of the projectile after collision differs from the groundstate showing a displacement of charge towards a region farther away from the nucleus (dark orange ring on the lower left hand side).

7 Conclusion

In summary, we report on the study of the collision of a gold atom impinging on a Au_{13} cluster, carried out by means of ab initio techniques. The minimum energy configurations of Au_{13} are almost planar and, for the time being, we have limited our interest to collisions where the projectile impacts orthogonally the cluster plane. The present work constitutes a new look at a problem treated some time ago by means of classical molecular dynamics [4] and the results turn out to be significantly different, which shows unambiguously that quantum effects cannot be ignored in these processes. This is due to the fact that classical computations do not include the possibility of charge transfer between the colliding atoms, which once included significantly favors fusion over fragmentation of projectile and cluster, in relation to classical molecular dynamics.

The dynamics of the collision is determined by the projectile kinetic energy and mainly by its impact parameter. Among the three regimes that we investigated in detail (fusion, scattering and fragmentation) and within the parameter space we investigated (i.e. the magnitude of the kinetic energy and the impact parameter) fusion is dominant and fragmentation the second most frequent outcome. Scattering instead is mainly the consequence of large impact parameter collisions and is of rather low occurrence.

By carrying out spin polarized calculations we also investigated the relevance that magnetic phenomena have in the proper description of cluster collision processes, finding out that the inclusion of magnetic effects leads to rather minor differences.

The rich diversity of the cluster structures generated by collisions strongly suggests that this type of treatment has the potential to be a powerful tool in the search of putative minimum energy cluster configurations.

Supported by the *Fondo Nacional de Investigaciones Científicas y Tecnológicas* (FONDECYT, Chile) under grants 1071062 and 1090225 (MK and JR), 1080239 (GG and RR), 1070854 (JAV) and *Financiamiento Basal para Centros Científicos y Tecnológicos de Excelencia*. FM and MR were supported by CONICYT scholarships.

References

1. W.A. de Heer, Rev. Mod. Phys. **65**, 611 (1993)
2. M. Valden, X. Lai, D.W. Goodman, Science **281**, 1647 (1998)
3. A.A. Herzing, C.J. Kiely, A.F. Carley, P. Landon, G.J. Hutchings, Science **321**, 1331 (2009)
4. J. Rogan, R. Ramírez, A.H. Romero, M. Kiwi, Eur. Phys. J. D **28**, 219 (2004)
5. S.M. Foiles, M.I. Baskes, M.S. Daw, Phys. Rev. B **33**, 7983 (1986)
6. N. Andersen, J.W. Gallagher, I.V. Hertel, Phys. Rep. **278**, 165 (1988)
7. N. Andersen, J.T. Broad, E.E.B. Campbell, J.W. Gallagher, I.V. Hertel, Phys. Rep. **278**, 107 (1997)
8. N. Andersen, K. Bartschat, J.T. Broad, I.V. Hertel, Phys. Rep. **279**, 251 (1997)
9. M. Kalweit, D. Drikakis, Phys. Rev. B **74**, 235415 (2006)
10. M.M. Mariscal, S.A. Dassie, E.P.M. Leiva, J. Chem. Phys. **123**, 184505 (2005)
11. D. Alamanova, V.G. Grigoryan, M. Springborg, J. Phys. Cond. Mat. **19**, 346204 (2007)
12. P. Hohenberg, W. Kohn, Phys. Rev. B **136**, 834 (1964)
13. W. Kohn, L.J. Sham, Phys. Rev. A **140**, 1133 (1965)
14. G. Kresse, J. Hafner, Phys. Rev. B **47**, 558 (1993)
15. G. Kresse, J. Furthmüller, Comput. Mater. Sci. **6**, 15 (1996)
16. G. Kresse, J. Furthmüller, Phys. Rev. B **54**, 11169 (1996)
17. G. Kresse, D. Joubert, Phys. Rev. B **59**, 1758 (1999)
18. J.P. Perdew, K. Burke, M. Ernzerhof, Phys. Rev. Lett. **77**, 3865 (1996)
19. J. Perdew, A. Zunger, Phys. Rev. B **23**, 5048 (1981)
20. J.P. Perdew, Y. Wang, Phys. Rev. B **45**, 13244 (1992)
21. M. Gruber, G. Heimel, L. Romaner, J. Bredas, E. Zojer, Phys. Rev. B **77**, 165411 (2008)
22. M. Mantina, R. Valero, D.G. Truhlara, J. Chem. Phys. **131**, 064706 (2009)
23. B.S. de Bas, M. Ford, M.B. Cortie, J. Phys. Cond. Mat. **18**, 55 (2006)
24. A. Vargas, G. Santarossa, M. Iannuzzi, A. Baiker, Phys. Rev. B **80**, 195421 (2009)
25. B. Assadollahzadeha, P. Schwerdtfegera, J. Chem. Phys. **131**, 064306 (2009)
26. Y. Dong, M. Springborg, Eur. Phys. J. D **43**, 15 (2006)
27. E.M. Fernández, J.M. Soler, I.L. Garzón, L.C. Balbás, Phys. Rev. B **70**, 165403 (2004)
28. M.P. Johansson, A. Lechtken, D. Schooss, M.M. Kappes, F. Furche, Phys. Rev. A **77**, 053202 (2008)
29. X. Li, H. Wang, X. Yang, Z. Zhu, J. Chem. Phys. **126**, 084505 (2007)
30. J. Wang, G. Wang, J. Zhao, Phys. Rev. B **66**, 035418 (2002)
31. L. Xiao, L. Wang, Chem. Phys. Lett. **392**, 452 (2004)
32. L. Xiao, B. Tollberg, X. Hu, L. Wang, J. Chem. Phys. **124**, 114309 (2006)
33. H. Häkkinen, M. Moseler, U. Landman, Phys. Rev. Lett. **89**, 033401 (2002)
34. J. Rogan, M. Ramírez, V. Muñoz, J.A. Valdivia, G. García, R. Ramírez, M. Kiwi, J. Phys. Cond. Mat. **21**, 084209 (2009)